

Discovery and Long-term Broadband X-ray monitoring of Galactic Black Hole Candidate MAXI J1803–298

MEGUMI SHIDATSU,¹ KOHEI KOBAYASHI,² HITOSHI NEGORO,² WATARU IWAKIRI,³ SATOSHI NAKAHIRA,⁴ YOSHIHIRO UEDA,⁵ TATEHIRO MIHARA,⁶ TERUAKI ENOTO,⁷ KEITH GENDREAU,⁸ ZAVEN ARZOUMANIAN,⁸ JOHN POPE,⁸ BRUCE TROUT,⁹ TAKASHI OKAJIMA,⁸ AND YANG SOONG⁸

¹*Department of Physics, Ehime University, 2-5, Bunkyocho, Matsuyama, Ehime 790-8577, Japan*

²*Department of Physics, Nihon University, 1-8-14 Kanda-Surugadai, Chiyoda-ku, Tokyo 101-8308, Japan*

³*Department of Physics, Faculty of Science and Engineering, Chuo University, 1-13-27 Kasuga, Bunkyo-ku, Tokyo 112-8551, Japan*

⁴*Institute of Space and Astronautical Science (ISAS), Japan Aerospace Exploration Agency (JAXA), 3-1-1 Yoshinodai, Chuo, Sagami, Kanagawa, 252-5210, Japan*

⁵*Department of Astronomy, Kyoto University, Kitashirakawa-Oiwake-cho, Sakyo-ku, Kyoto, Kyoto 606-8502, Japan*

⁶*High Energy Astrophysics Laboratory, RIKEN, 2-1, Hirosawa, Wako, Saitama 351-0198, Japan*

⁷*RIKEN Cluster for Pioneering Research, 2-1 Hirosawa, Wako, Saitama 351-0198, Japan*

⁸*Astrophysics Science Division, NASA Goddard Space Flight Center, Greenbelt, Maryland 20771, USA*

⁹*Microtel, Greenbelt, MD 20770, USA*

ABSTRACT

We report the results from the broad-band X-ray monitoring of the new Galactic black hole candidate MAXI J1803–298 with the MAXI/GSC and *Swift*/BAT during its outburst. After the discovery on 2021 May 1, the soft X-ray flux below 10 keV rapidly increased for ~ 10 days and then have been gradually decreasing over 5 months. At the brightest phase, the source exhibited the state transition from the low/hard state to the high/soft state via the intermediate state. The broad-band X-ray spectrum during the outburst was well described with a disk blackbody plus its thermal or non-thermal Comptonization. Before the transition the source spectrum was described by a thermal Comptonization component with a photon index of ~ 1.7 and an electron temperature of ~ 30 keV, whereas a strong disk blackbody component was observed after the transition. The spectral properties in these periods are consistent with the low/hard state and the high/soft state, respectively. A sudden flux drop with a few days duration, unassociated with a significant change in the hardness ratio, was found in the intermediate state. A possible cause of this variation is that the mass accretion rate rapidly increased at the disk transition, which induced a strong Compton-thick outflow and scattered out the X-ray flux. Assuming a non-spinning black hole, we estimated a black hole mass of MAXI J1803–298 as $5.8 \pm 0.4 (\cos i / \cos 70^\circ)^{-1/2} (D/8 \text{ kpc}) M_\odot$ (where i and D are the inclination angle and the distance) from the inner disk radius obtained in the high/soft state.

Keywords: X-rays: individual (MAXI J1803–298) — X-rays: binaries — accretion, accretion disks — black hole physics

1. INTRODUCTION

Most of the known Galactic black hole X-ray binaries (BHXB) exhibit transient behaviors. They are usually dormant in X-rays but suddenly enter into an outburst, increasing their X-ray luminosities by several orders of magnitude. Because the X-rays are produced in the in-

ner parts of the accretion disk, through the release of gravitational energy of the accreted gas, the X-ray luminosity and energy spectrum depend on the mass accretion rate and the structure of the inner disk, and the spacetime in the vicinity of the black hole. X-ray observations of BHXBs therefore give clues to understanding black hole accretion flows and the nature of the black holes themselves. In particular, monitoring broadband X-ray spectra during their outbursts is helpful to study the evolution of the accretion flows over a wide range of mass accretion rates.

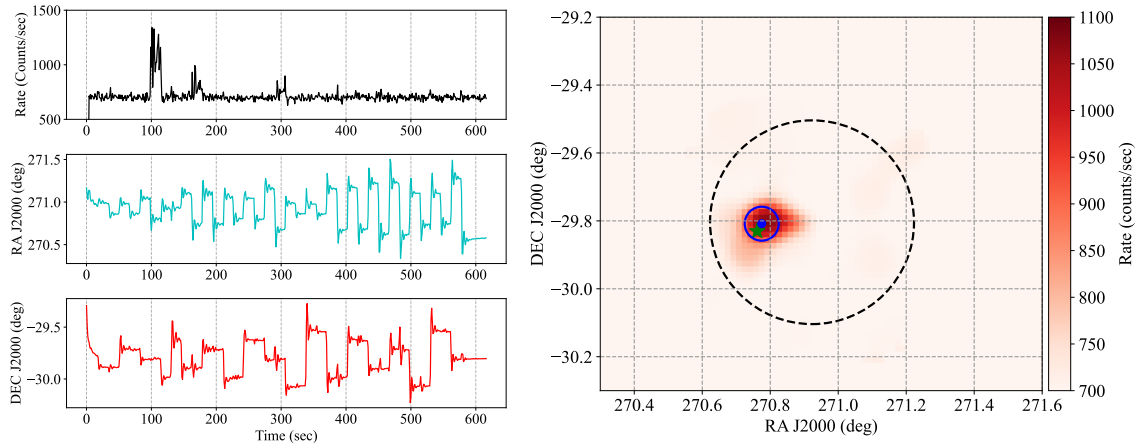


Figure 1. (Left) Time evolution of the NICER raw counts and the pointing direction in R.A. and Dec obtained by the NICER multiple pointings of MAXI J1803–298. (Right) 2D histogram of the NICER count rate map (see text). The black dotted circle indicates the error circle of the MAXI data reported by Serino et al. (2021). The blue filled circle indicates the location of the pixel with the maximum count rate, and the blue solid circle around it represents the FoV of NICER. The green filled star denotes the MAXI J1803–298 position determined by *Swift* (Gropp et al. 2021).

The Galactic black hole candidate MAXI J1803–298 was discovered on 2021 May 1 (Serino et al. 2021) with the nova search system (Negoro et al. 2016) of MAXI (Matsuoka et al. 2009). Its position was then localized by the NICER multiple pointings (Gendreau et al. 2021) and further constrained with *Swift* (Gropp et al. 2021). Follow-up observations were performed many times in X-rays (Sguera & Sidoli 2021; Chenevez et al. 2021; Bult et al. 2021; Homan et al. 2021; Xu & Harrison 2021; Miller & Reynolds 2021; Wang et al. 2021; Shidatsu et al. 2021; Jana et al. 2021; Chand et al. 2021; Ubach et al. 2021; Steiner 2021; Chand et al. 2021; Feng et al. 2021) and other wavelengths (Hosokawa et al. 2021; Buckley et al. 2021; Espinasse et al. 2021; Saikia et al. 2021; Mata Sánchez et al. 2022). NuSTAR and NICER found periodic absorption dips, and *Swift* detected absorption lines likely originating in a disk wind (Miller & Reynolds 2021), both suggestive of a high inclination angle above $\sim 70^\circ$. A sign of an outflow was also detected in optical spectroscopy (Buckley et al. 2021), where p Cygni-like profiles were detected in hydrogen Balmer lines.

In this article, we report the results from long-term, broadband X-ray monitoring of MAXI J1803–298 over the almost entire outburst, using the *MAXI*/Gas Slit Camera (GSC) and *Swift*/Burst Alert Telescope (BAT) data. We used Heasoft version 6.28 and XSPEC version 12.11.1 for data reduction and analysis, and adopted the solar abundance table given by Wilms et al. (2000). Throughout the article, errors represent the 90% confidence ranges for one parameter, unless otherwise specified.

2. OBSERVATIONS AND DATA REDUCTION

2.1. Localization of the MAXI J1803–298 position

At 19:50 UT on 2021 May 1, the MAXI/GSC nova search system triggered an uncatalogued X-ray transient source. The source position determined by MAXI was $(\alpha^{2000}, \delta^{2000}) = (18^h 03^m 41^s, -29^\circ 48' 14'')$ with a statistical error of about ± 0.3 deg and a systematic uncertainty of ± 0.1 deg. Following the MAXI alert of a new transient, NICER performed multiple pointings to localize the source position from 03:36 UT on 2021 May 2 using the non-imaging NICER/XTI. Starting from the nominal coordinates reported by MAXI, NICER performed 37 offset pointings with a step interval of 6 arcmin, which is the same as the size of NICER’s field of view (FoV). The exposure time for each pointing was about 15 seconds. Figure 1 (left) shows the time evolution of the NICER raw counts and the pointing direction coordinates, whereas Figure 1 (right) shows the count rate map created from the raw counts and exposure time map. The vignetting effect in the each pointing was corrected using the vignetting profile of the NICER X-ray concentrator obtained from ray-tracing simulations that considered calibration test results obtained with the 1.5 keV X-rays at the NASA/GSFC 100-m X-ray beamline. The image was smoothed with a Gaussian filter of standard deviation of 1 pixel (1 arcmin). The coordinates of the source estimated from the maximum value of the count rate map is $(\alpha^{2000}, \delta^{2000}) = (18^h 03^m 09^s, -29^\circ 48' 43'')$. After further follow-up observations by *Swift* (Gropp et al. 2021), the position of MAXI J1803–298 was determined to be $(\alpha^{2000}, \delta^{2000}) = (18^h 03^m 02^s.79, -29^\circ 49' 49.''7)$,

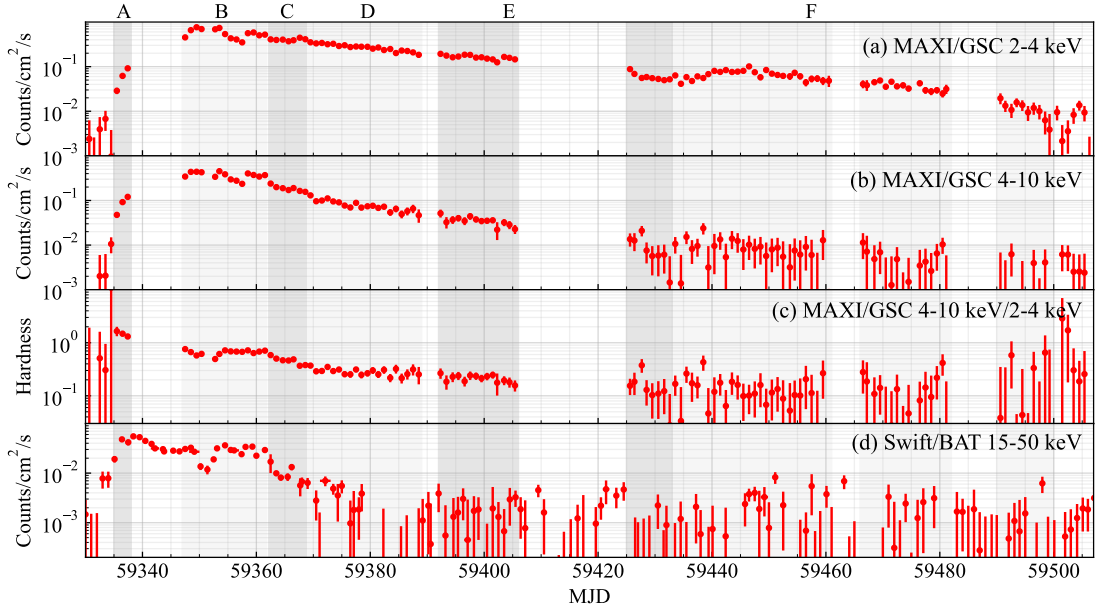


Figure 2. 2–4 keV and 4–10 keV *MAXI*/GSC light curves of MAXI J1803–298, their hardness ratio, and the *Swift*/BAT 15–50 keV light curve, from top to bottom. All the data points are binned into 1-day intervals. The error bars indicate 1σ statistical errors. The phases given in Tab. 1 are also indicated.

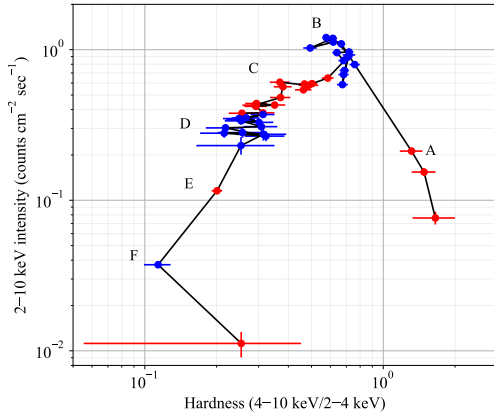


Figure 3. Hardness intensity diagram of MAXI J1803–298, produced with the *MAXI* data in Fig. 2(a)–(c). The phases given in Tab. 1 are indicated. The data points in Phase E, F, and the later phase (MJD 59500–59506) are averaged for each phase, to improve statistics.

or $(l, b) = (1^\circ.147184, -3^\circ.727501)$. This is consistent with the coordinates obtained from the *NICER* multiple pointing observation within their field of view of 3 arcmin radius.

2.2. *MAXI*

MAXI has been monitoring MAXI J1803–298 since its discovery on 2021 May 1 (MJD 59335). In this work,

we used all the available GSC data taken from 2021 April 26 (MJD 59330) to October 19 (MJD 59506). We produced *MAXI*/GSC long-term light curves through a point-spread-function (PSF) fit method (Mori et al. 2010). To extract the GSC spectra, we utilized the *MAXI* on-demand software (Nakahira et al. 2013) and the Calibration Database (CALDB) latest as of 2021 May. The source and background extraction regions were defined as a circle with a 1.6° radius and an annulus within radii from 1.7° to 3° , respectively, both centered at the source position.

Although the source region includes the neighbouring source XTE J1807–294 located 0.96° apart, its contamination is likely to be negligible. To evaluate the contamination flux level from XTE J1807–294, we extracted the time-averaged spectrum for 1 year before the discovery (MJD 58970–59334) from the same source region. However, we did not detect source signals significantly, and obtained an upper limit for the 2–10 keV flux of 0.8 mCrab (2.4×10^{-11} erg cm $^{-2}$ s $^{-1}$), assuming the Crab spectrum ($\Gamma = 2.1$, $N_{\text{H}} = 3 \times 10^{21}$ cm $^{-2}$). This is a negligible level in our analysis. To avoid source contamination to the background data, we excluded, from the background region, areas within certain radii (depending on the source fluxes) around the nearby bright sources: 1.0° , 1.5° , 1.8° , 1.4° , and 2.3° around SAX J1747.0–2853, 1A 1742–294, XTE J1751–305, H 1755–338, and GX 5–1, respectively, all of which are

located 3.5° – 5.0° apart from MAXI J1803–298. We determined these exclusion radii based on the 2–10 keV GSC image in MJD 59335–59350 obtained with the on-demand software, so that the PSFs of the sources were sufficiently covered.

2.3. *Swift*

We also used the *Swift*/BAT survey-mode data for the same period as the MAXI/GSC data. The BAT data were downloaded from the HEADAS archive¹, and were reduced with the *Swift*/BAT CALDB released on 2017 October 16. The data were first processed with the `ftool batsurvey`. The tool produces files that list the count rates of the sources in the BAT field of view for the individual scans. From these products we calculated the 1-day averaged count rates of MAXI J1803–298 using the `ftool ftcalc` and compiled them into a light curve. The time-averaged spectrum and the response file for each continuous scan were produced with the dedicated script `make_survey pha` from the `batsurvey` products. We created time-averaged spectra for longer time intervals by merging the spectra and response files via `ftools mathpha` and `addrmf` and used them in the spectral analysis (see Sec. 4). In this analysis, we discarded the spectral bins when only upper limits on the count rates were obtained.

3. LIGHT CURVES AND HARDNESS-INTENSITY DIAGRAM

Figure 2 presents the MAXI light curves and hardness ratios, and *Swift*/BAT hard X-ray light curve of MAXI J1803–298. In the initial phase of the outburst, the source flux rapidly increased by ~ 2 orders of magnitude. The *Swift*/BAT data suggest that the outburst started at least a few days before the discovery with the MAXI/GSC on MJD 59335. After the source was out of MAXI’s field of view from MJD 59338 to MJD 59346, it reached the peak with ~ 0.6 Crab in 2–4 keV and ~ 0.4 Crab in 4–10 keV. The hardness ratio dropped in this data gap, suggesting that the source started the state transition from the low/hard state to the high/soft state, as reported by Shidatsu et al. (2021). The *Swift*/BAT hard X-ray flux reached its peak around MJD 59339, ~ 10 days before the flux peak below 10 keV. After the flux peaks, the source has gradually dimmed over 5 months, with a slight rebrightening around MJD 59440. Using the NICER data, Steiner (2021) reported that the source returned to the low/hard state between MJD 59500 and MJD 59506, although this transition is not very clear in Fig. 2 due to low statistics.

¹ <https://heasarc.gsfc.nasa.gov/FTP/swift/data/obs/>

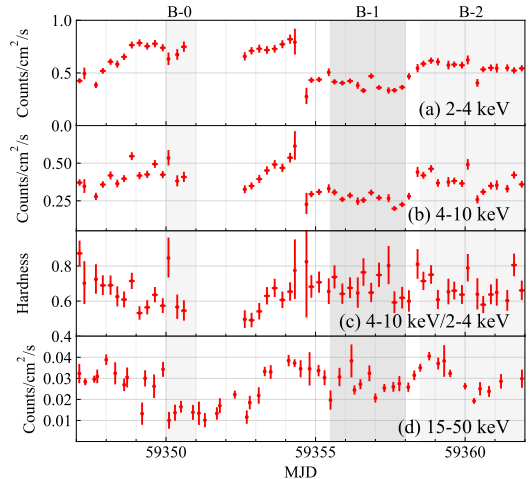


Figure 4. Same as Fig. 2, but with 6-hour bins and limited in MJD 59345–59362 (Phase-B). The shadowed regions indicate the phases of the highest soft X-ray flux with relatively weak hard X-rays (Phase B-0), the flux drop in the soft X-rays (Phase B-1), and after the drop (Phase B-2), used in Section 4.2.

Table 1. List of phases.

ID	State	Period	Exposure	
		(MJD)	GSC (cm^2 ks)	BAT (ks)
A	low/hard	59335–59337	7.9	22
B	intermediate	59347–59361	31.9	175
C	high/soft	59362–59375	20.3	109
D	high/soft	59376–59389	16.6	98
E	high/soft	59393–59432	36.8	400
F	high/soft	59433–59500	89.7	657

In Figure 3 we plot the hardness intensity diagram, where a counter-clockwise path is seen like other transient BHXBs. On the basis of the behavior of the source fluxes and hardness ratio, we defined six phases listed in Table 1 and used them in the following spectral analysis. Here, the data gaps of MAXI/GSC were omitted. The data before the discovery (until MJD 59334) and after MJD 59500 were also ignored, because we were unable to obtain statistically meaningful spectra due to the too low flux. Considering the hardness intensity diagram, the source was likely to be in the low/hard state and the high/soft state in Phases A and C–F, respectively, in which the source had a high and low hardness ratios. In Phase B, the hardness ratio was between the values in Phases A and C–F, indicating that the source was likely

to be in the intermediate state. These are confirmed in the following spectral analysis.

We also created 6-hour bin light curves (Figure 4) in Phase B to study variability during the intermediate state. Interestingly, the source exhibited a flux drop by $\sim 40\%$ during MJD 59355–59358 without changing the level of the hardness ratio significantly. In addition, the *Swift*/BAT hard X-ray flux was dropped by 60% around the soft X-ray peak (MJD 59350).

4. SPECTRAL ANALYSIS AND RESULTS

4.1. Time-averaged Spectra in the individual phases

Figure 5 shows the time-averaged MAXI/GSC and *Swift*/BAT spectra in the individual phases. For the MAXI/GSC data, we discarded the spectral bins at high energies when the source count rate is below $\sim 10\%$ of the background level. In Appendix A, we show the MAXI/GSC response folded spectra and their background contribution. The *Swift*/BAT data for Phase D, E, and F, was unavailable. In these phases, all of the spectral bins gave only upper limits on the count rates. In Phase A, the source exhibited a hard, power-law shaped spectrum with a cutoff at ~ 50 keV. Then, in Phase B, a strong thermal component, likely originated in the standard disk, emerged in the soft X-ray band. Meanwhile, the spectral cutoff disappeared in the hard X-ray band. A strong, steep power-law shaped component, with a photon index of ~ 2.5 , was seen in the Phase B spectrum, while in later phases the hard X-ray component became weak and harder.

We analyzed the broad-band X-ray spectra of MAXI J1803–298 using a standard model for BHXBs: the multi-color disk blackbody emission (`diskbb`; Mitsuda et al. 1984) and its Comptonization. The `diskbb` model is parametrized by the disk temperature and the normalization that is determined by the inner disk radius r_{in} , the distance D , and the inclination angle i . For the Comptonization component, we adopted `nthcomp` for Phase A (Zdziarski et al. 1996; Życki et al. 1999) and `simpl` (Steiner et al. 2009) for Phase B–F. The `nthcomp` model calculates a thermally Comptonized spectrum using the photon index Γ , the electron temperature kT_e , and seed photon temperature (the inner disk temperature kT_{in} when the seed spectrum is set to be a disk blackbody). Because the direct disk component is not seen in the soft X-ray band, the `diskbb` model was not used and kT_{in} was fixed at 0.1 keV for the Phase-A spectrum. The `simpl` model is a convolution model redistributing a fraction (F_{scat}) of the input seed photons into a power-law profile with a photon index Γ . When using this model, we extended the energy range used in the calculation down to 0.01 keV and up to 1000 keV so

that the spectral fit is not affected by uncertainties at the upper and lower boundaries of energy.

We also used the `TBabs` model to account for the interstellar absorption. Since the MAXI/GSC has sensitivity only above 2 keV, it is difficult to determine the column density. The column density was therefore fixed at $N_{\text{H}} = 3 \times 10^{21} \text{ cm}^{-2}$, which was obtained in a NICER observation (Homan et al. 2021). We have confirmed that the uncertainty in N_{H} gives only a small effect to the fit parameters; they do not change beyond their 90% error ranges when $N_{\text{H}} = 2 \times 10^{21} \text{ cm}^{-2}$ and $N_{\text{H}} = 4 \times 10^{21} \text{ cm}^{-2}$ were adopted. The cross-normalization factor of the *Swift*/BAT data with respect to the MAXI/GSC data was varied to account for the uncertainty in the instrumental cross calibration and that caused by flux variation.

Homan et al. (2021), Xu & Harrison (2021), and Jana et al. (2021) reported that the source showed strong absorption dips, with a ~ 7 -hour interval and a ~ 5000 s duration, in which the X-ray intensity was reduced by ~ 50 – 100% . However, we found that the effect in our spectral analysis was negligible. The conclusion of the analysis did not change when the data in the dip phases (assuming the above interval and duration, and the center of a dip reported by Homan et al. 2021) were excluded. This is likely because the strong dips were short-lived compared with the data periods that we employed. Actually, previous studies of other transient BHXBs found that dips were seen only a limited period of outbursts (e.g., Kuulkers et al. 2013).

As shown in Fig. 5, the `TBabs*nthcomp` model and `TBabs*simpl*diskbb` model were able to reproduce the observed spectra. The best-fit parameters in each phase are summarized in Table 2. The phase C–F spectra were dominated by the `diskbb` component in the soft X-ray band below 10 keV. In Phase D–F, the photon index Γ was not constrained at all, because the hard tail was not clearly observed due to the lack of the hard X-ray data. For these phases, we adopted the best-fit value in phase C, $\Gamma = 2.1$. Many previous works of BHXBs indicated that the inner disk radius remains constant when the X-ray spectrum is dominated by disk blackbody emission (e.g., Ebisawa et al. 1993; Kubota & Makishima 2004; Steiner et al. 2010; Shidatsu et al. 2011). Considering this, we attempted to fit the Phase C–F spectra simultaneously, linking the `diskbb` normalizations of all the phases. In this fit, Γ was also linked to one another. As shown in Tab. 2, we obtained an acceptable fit, which gave $r_{\text{in}} = 44 \pm 3 (\cos i / \cos 70^\circ)^{-1/2} (D/8 \text{ kpc}) \text{ km}$.

4.2. Short-term Variation in Phase B

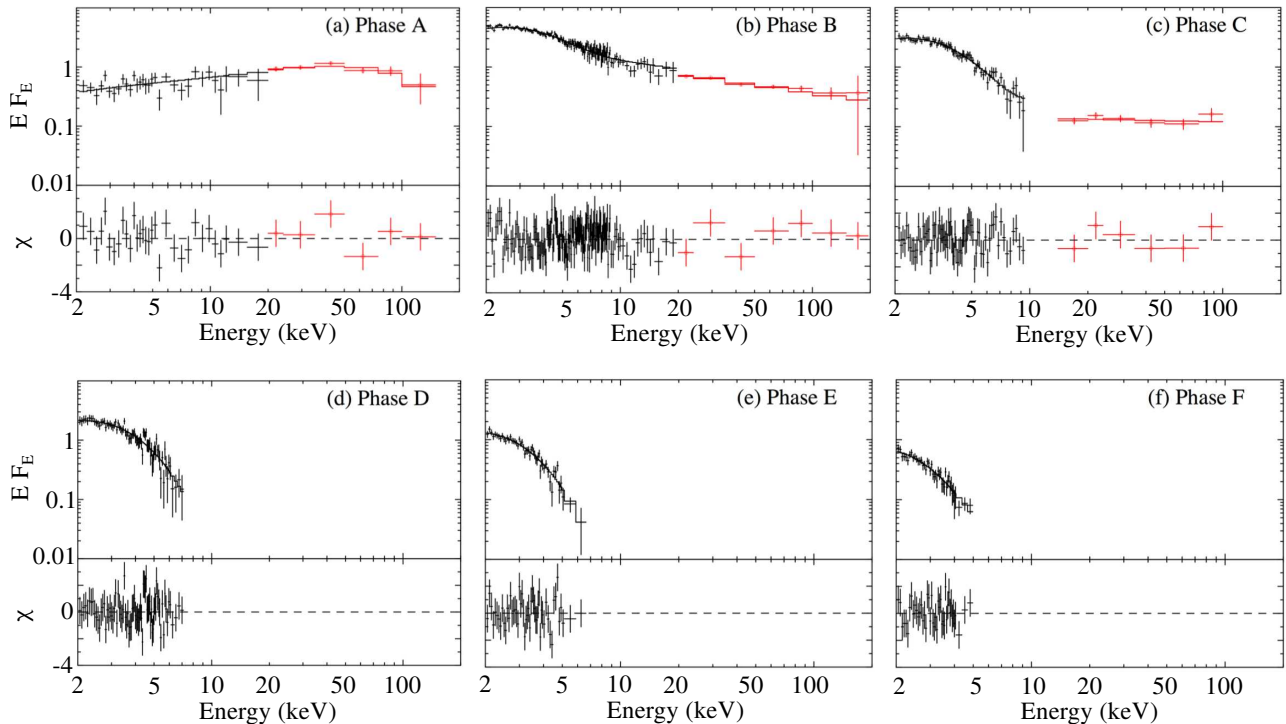


Figure 5. (Top) unfolded *MAXI*/GSC (black) and *Swift*/BAT (red open square) spectra for the individual phases given in Tab. 1, fitted with the `TBabs*nthcomp` model (for Phase A) or `TBabs*simpl*diskbb` model (Phase B–F). The units of the ordinate axes are $\text{keV} (\text{Photons cm}^{-2} \text{s}^{-1} \text{keV}^{-1})$. (Bottom) Residuals for the best-fit models.

Next, to study the spectral variation in the intermediate state, we made 1-day averaged *MAXI*/GSC and *Swift*/BAT spectra in Phase B and applied the same model as in Sec. 4.1: the `TBabs*simpl*diskbb` model. The model successfully reproduced all the data. Figure 6 shows two representative spectra at different X-ray fluxes and their best-fit models, and Figure 7 presents the time variation of the best-fit parameters. At the brightest phase in soft X-rays (around MJD 59350; hereafter we call Phase B-0), the spectrum was dominated by the thermal component below 10 keV and the hard tail had a photon index of ~ 2.0 , while a steep power-law shaped spectrum with a photon index of 2.3–2.7 was seen at the other time periods in Phase B.

To investigate the cause of the flux drop seen in Fig. 4, we also made time-averaged spectrum in MJD 59355.5–59358.0 (during the deepest flux drop; hereafter we call Phase B-1) and in MJD 59358.5–59362.0 (after the drop; Phase B-2), and applied the same spectral model as above. The two spectra and their best-fit model are shown in Figure 8, and the best-fit parameters are given in Table 2. We found that T_{in} was lower in the Phase B-1 than in Phase B-2. By contrast, r_{in} and F_{scat} favored larger values in Phase B-1, although they were marginally consistent each other between the two phases when the 90% uncertainties were considered.

The bottom panel in Figure 8 shows the ratio of the raw spectra folded by the instrumental responses. The Phase B-1 spectrum has a slightly larger soft X-ray fraction below 3 keV than the Phase B-2 spectrum, which is consistent with the change in T_{in} . We note that this flux drop cannot be explained by the increase in the absorption column density alone. In such case, softer X-rays would be more strongly absorbed and thus the spectrum would become significantly harder in the flux drop. To test if the absorption can explain at least some fraction of the flux drop at low energies, we fit the spectra with the same model above, allowing N_{H} to vary. The fit only gave upper limits, $N_{\text{H}} \sim 4 \times 10^{21} \text{ cm}^{-2}$, for both spectra, but this value suggests that the absorption was not strongly enhanced in the flux drop.

5. DISCUSSION

5.1. Long-term Evolution and Spectral States

We have performed long-term X-ray monitoring of the new Galactic black hole candidate *MAXI* J1803–298 over 5 months since its discovery, using the *MAXI*/GSC and *Swift*/BAT. The long-term light curves were characterized by a rapid rise and slow decay, and the spectral softening was observed at the brightest phase (Fig. 2). In the hardness intensity diagram, the source drew a counter-clockwise path (Fig. 3) like other transient BHXBs (e.g., Miyamoto et al. 1995). Re-

Table 2. Best-fit spectral parameters^a in each phase.

Phase	Γ	kT_e	F_{scat}	kT_{in}	r_{in}^b	cross norm.	χ^2/dof	F_X^c
		keV		keV	km	BAT/GSC		$10^{-9} \text{ erg s}^{-1} \text{ cm}^{-2}$
A	1.7 ± 0.1	26_{-7}^{+18}	—	0.1 (fixed)	—	$1.0_{-0.2}^{+0.3}$	38/35	$5.5_{-0.5}^{+0.6}$
B	$2.46_{-0.07}^{+0.08}$	—	$0.22_{-0.02}^{+0.03}$	0.88 ± 0.03	46_{-3}^{+4}	0.8 ± 0.1	155/154	19.8 ± 0.5
C	2.1 ± 0.2	—	0.04 ± 0.02	0.86 ± 0.04	40 ± 4	$0.5_{-0.2}^{+0.4}$	65/77	$11.7_{-0.7}^{+0.8}$
D	2.1 (fixed)	—	< 0.03	$0.81_{-0.06}^{+0.03}$	38_{-3}^{+7}	—	77/75	$7.5_{-0.4}^{+0.9}$
E	2.1 (fixed)	—	< 0.02	$0.64_{-0.03}^{+0.02}$	50_{-3}^{+7}	—	52/49	$4.8_{-0.2}^{+0.7}$
F	2.1 (fixed)	—	< 0.04	$0.56_{-0.07}^{+0.04}$	42_{-6}^{+17}	—	30/41	$2.1_{-0.3}^{+0.6}$
B-1	2.7 ± 0.2	—	> 0.3	< 0.72	93_{-34}^{+930}	1.1 ± 0.3	46/33	$17.5_{-1.9}^{+7.7}$
B-2	2.5 ± 0.1	—	$0.26_{-0.04}^{+0.05}$	0.85 ± 0.06	51_{-6}^{+8}	0.8 ± 0.1	38/35	$21.7_{-0.9}^{+1.0}$
(Simultaneous fit)								
C	2.1 ± 0.2^d	—	$0.05_{-0.01}^{+0.02}$	0.83 ± 0.02	44 ± 3^d	$0.5_{-0.1}^{+0.2}$	234/245 ^e	$11.7_{-0.7}^{+0.8}$
D	(linked)	—	$0.019_{-0.018}^{+0.019}$	0.77 ± 0.02	(linked)	—	...	$7.5_{-0.4}^{+1.0}$
E	(linked)	—	$< 5 \times 10^{-3}$	$0.67_{-0.01}^{+0.02}$	(linked)	—	...	$5.0_{-0.3}^{+0.4}$
F	(linked)	—	$< 3 \times 10^{-2}$	$0.56_{-0.02}^{+0.01}$	(linked)	—	...	$2.2_{-0.3}^{+0.6}$

^aThe `TBabs*nthcomp` model was applied for Phase A, while `TBabs*simpl*diskbb` was adopted to the other phases. The N_{H} value of `TBabs` was fixed at $3.0 \times 10^{21} \text{ cm}^{-2}$.

^bInner disk radius estimated from the relation $r_{\text{in}} = \sqrt{N_{\text{dbb}}/\cos i} (D/10 \text{ kpc})$, where N_{dbb} , D , and i are distance and inclination angle, respectively. $i = 70^\circ$ and $D = 8 \text{ kpc}$ were assumed here.

^cUnabsorbed 0.01–100 keV flux.

^dThe normalizations of `diskbb` and Γ of `simpl` were linked among the four phases.

^eTotal $\chi^2/\text{d.o.f.}$ value of all the four spectra.

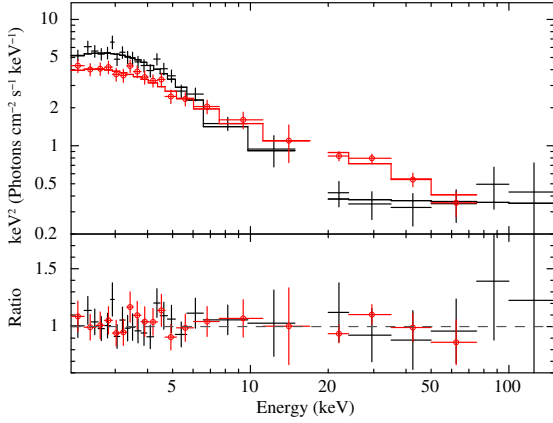


Figure 6. One-day-averaged unfolded spectra taken on MJD 59347 (red open circles) and MJD 59350 (Phase B-0; black crosses) and their best-fit `TBabs*simpl*diskbb` models (top) and the data versus model ratio (bottom).

cently, the soft-to-hard transition was reported, from NICER observations, to have occurred between MJD 59500 and 59506 (Steiner 2021). The low statistics of the MAXI/GSC data hampered the determination of the exact time of the transition, but the hardness inten-

sity diagram suggests that the luminosity of the soft-to-hard transition was ~ 1 order of magnitude lower than that of the opposite transition.

The combination of the two instruments enabled us to study the broad-band X-ray spectrum in 2–200 keV and its evolution during the outburst. At the initial rise of the soft X-ray flux (Phase A), the source showed a typical low/hard state spectrum. The spectrum was well reproduced with a thermal Comptonization with $\Gamma \sim 1.7$ and $T_e \sim 30 \text{ keV}$, and the direct disk emission component was not observed. At the highest flux phase (Phase B), the soft X-ray fraction increased and the time-averaged spectrum was characterized by a steep power-law model with $\Gamma \sim 2.5$ consistent with the spectral profile in the intermediate or very high state. Although previous studies suggest disk truncation in this state (Tamura et al. 2012; Hori et al. 2014), we did not detect a significant increase in r_{in} likely due to the insufficient quality of the data. We note that the r_{in} values obtained from the `simpl*diskbb` model include the contributions of the scattered disk photons.

Due to the data gap of the MAXI/GSC, it is unclear exactly when is the onset of the transition, but most

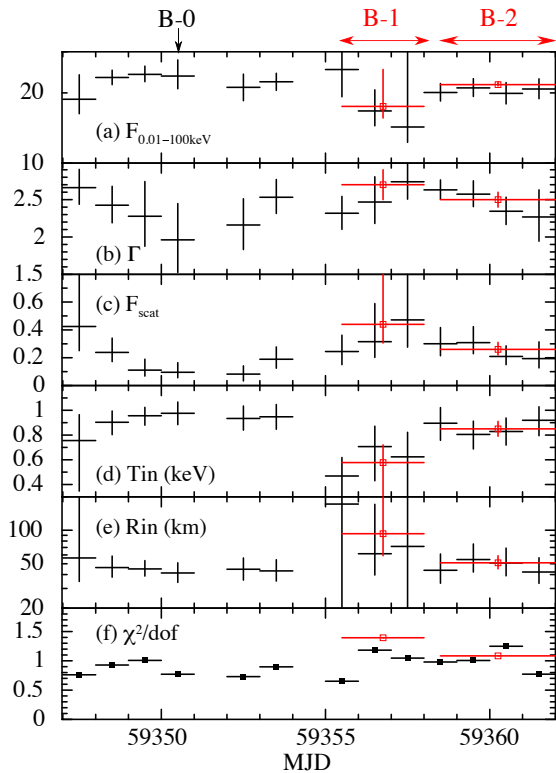


Figure 7. Time variations of the best-fit spectral parameters in the intermediate state (Phase B). The top panel plots the unabsorbed 0.01–100 keV flux in units of 10^{-9} erg cm^{-2} s^{-1} . Results from the 1-day averaged spectra are shown in black and those from the Phase B-1 and B-2 spectra in red (with open squares).

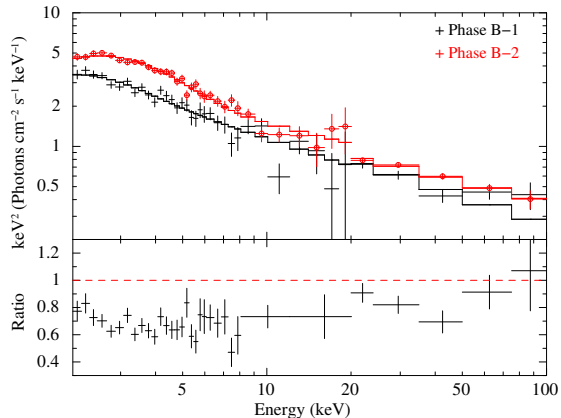


Figure 8. (Top) Time-averaged unfolded spectra in Phase B-1 (black crosses) and B-2 (red open circles) and their best-fit models. (Bottom) Ratio of the folded spectrum in Phase B-1 with respect to that in Phase B-2. The data points in 8–20 keV are binned further for visual purposes.

likely it occurred around the middle of the data gap of the MAXI/GSC; NuSTAR observed a typical low/hard state spectrum on MJD 59339–59340 (Xu & Harrison 2021) while on MJD 59345–59346, AstroSAT detected a

significant disk blackbody component with an inner disk temperature of ~ 0.6 keV, suggesting that the source was already in the intermediate state (Jana et al. 2021). We have investigated the 1-day averaged *Swift*/BAT spectra in the data gap of MAXI, but detected no significant spectral variation due to low statistics.

At the decaying phase after the intermediate state (Phase C–F), the spectrum was described by dominant multi-color disk blackbody emission in the soft X-ray band and a weak power-law tail with $\Gamma \sim 2.0$ in the hard X-ray band. These spectral properties are consistent with the high/soft state. Applying the disk blackbody and its non-thermal Comptonization model, we obtained the inner disk temperature $T_{\text{in}} \sim 0.5\text{--}1$ keV and the scattering fraction $F_{\text{scat}} < 10\%$, in agreement with typical BHXBs in the high/soft state (McClintock & Remillard 2006). Unlike the case of neutron star low mass X-ray binaries, no additional blackbody component was required in this period, supporting the black hole nature of the source. The idea that the source contains a black hole is consistent with the fact that no coherent pulsation has been detected so far (e.g., Xu & Harrison 2021). We note that search for pulsation using the MAXI/GSC data is difficult, because of the insufficient statistics and the very large time gap between each scan (MAXI observes a source for only a few minutes in a 92 minute orbit; see Sugizaki et al. 2011). Systematic search for pulsation of MAXI J1803–298 is beyond our scope and we leave it as a future work. We have also searched the MAXI 2–10 keV light curve over the entire outburst period but found no X-ray bursts. This also indirectly supports the black hole nature.

5.2. Variation in the Intermediate State

Significant spectral variation on timescales of \sim day was observed in the intermediate state (Phase B). Around Phase B-0, which corresponds to the flux peak in the soft X-ray band, the spectrum was characterized by a dominant thermal disk component and a relatively weak hard tail with $\Gamma \sim 2.0$, reminiscent of the high/soft state spectrum. At lower luminosities, the source exhibited a steep power-law shaped spectrum with $\Gamma \sim 2.5$, consistent with the very high state spectrum, which is normally seen at higher luminosity than that in the high/soft state. Given that the steep power-law spectrum usually seen at sub-Eddington luminosities ($0.2\text{--}1 L_{\text{Edd}}$, where L_{Edd} is the Eddington luminosity), the source luminosity may have exceeded L_{Edd} at Phase B-0 and made the transition in the inner disk region from the standard disk to the slim disk. Using the best-fit `simpl*diskbb` model, we estimated the unabsorbed 0.01–100 keV flux at this phase of $\sim 2.4 \times 10^{-8}$ erg cm^{-2}

s^{-1} . If the source had $\sim 1L_{\text{Edd}}$ at this epoch, the unabsorbed 0.01–100 keV luminosity in Phase F is estimated to be $\sim 0.1L_{\text{Edd}}$. This is higher than the typical transition luminosity from the high/soft state to the low/hard state, $\sim 1\%$ – 4% L_{Edd} (Maccarone 2003; Vahdat Motlagh et al. 2019), and therefore suggests that the transition to the low/hard state should occur after Phase F. Indeed, a high/soft state spectrum was observed in Phase F and Steiner (2021) reported that the transition took place after Phase F.

In addition, we found a sudden flux drop with a duration of a few days, when the steep power-law spectrum was observed. Remarkably, the hardness ratio between the 4–10 keV and 2–4 keV fluxes remained almost constant in this period (Fig. 4). Comparing the spectra during and after the flux drop in detail, we found that the fraction of the flux around ~ 2 keV is slightly enhanced during the dip. Application of the `simpl*diskbb` model yielded a smaller inner disk temperature and marginally larger inner disk radius and scattering fraction during the flux drop than after the drop.

What produced this variation? One possibility is that the standard disk was truncated outside the innermost stable circular orbit (ISCO), and the transition from the standard disk to a strongly Comptonized accretion flow was taking place in the innermost region of the remaining disk (Tamura et al. 2012; Hori et al. 2014). Such a transition, however, would progress as the mass accretion rate goes up. This contradicts what we observed: the disk receded as X-ray flux decreased. Another possibility would be that the mass accretion rate rapidly increased. In this case, the inner disk region may become geometrically thicker and reduce the apparent flux by shielding a part of the disk, although it is unclear whether the spectral shape can be kept almost constant. If the mass accretion rate goes up beyond the Eddington limit, a massive outflow can be launched in the inner disk region. If such outflow was really launched and was Compton thick and almost completely ionized, strong scattering could reduce the apparent X-ray flux without a great change in the spectral shape. A candidate of the Compton-thick wind was actually observed in GRO J1655–40 at similar luminosities (Shidatsu et al. 2016; Neilsen et al. 2016).

We note, however, that the very high state spectra are more complex than the `simpl*diskbb` model (e.g., Gierliński & Done 2003; Tamura et al. 2012; Hori et al. 2014) and the spectral parameters that we estimated are taken with caution. Application of more realistic models to higher quality broad-band spectra would be required to investigate the details of the accretion flow structure at this epoch.

5.3. Constraint on the Black Hole Mass

Previous studies suggested that the standard disk extends stably down to the ISCO in the high/soft state. Since the ISCO depends on the mass of the central compact object, we can constrain the black hole mass of MAXI J1803–298 from the inner disk radius estimated in the high/soft state. In our spectral analysis, we obtained $r_{\text{in}} = 44 \pm 3 (\cos i / \cos 70^\circ)^{-1/2} (D/8 \text{ kpc}) \text{ km}$, from the normalization of `diskbb`. Considering the correction factor of the boundary condition at the inner disk edge and the color-temperature correction factor (K in total), the actual inner radius was estimated to be $R_{\text{in}} = Kr_{\text{in}} = 52 \pm 4 (\cos i / \cos 70^\circ)^{-1/2} (D/8 \text{ kpc}) \text{ km}$. Here we adopted $K = 1.19$, assuming a color-temperature correction factor (f_{col}) of 1.7 (Shimura & Takahara 1995) and a torque-free inner boundary (Kubota et al. 1998). Assuming a Schwarzschild black hole, we obtain a black hole mass of $M_{\text{BH}} = 5.8 \pm 0.4 (\cos i / \cos 70^\circ)^{-1/2} (D/8 \text{ kpc}) M_{\odot}$.

In the above discussion, we only considered the 90% error of r_{in} obtained in the spectral fit, but the color-temperature correction factor could be an additional source of uncertainty. Davis et al. (2005) obtained $f_{\text{col}} = 1.4$ – 1.7 from the calculation of the disk spectrum considering radiation transfer in the disk atmosphere and comparison with observations. If we adopt the lowest value, 1.4, K is reduced by $\sim 30\%$ and thereby M_{BH} decreases by the same factor. Another uncertainty could be posed by the relativistic effects, which is not considered in the `diskbb` model. To investigate the effects, we fit the Phase C–F spectra simultaneously in the same manner as in Section 4.1, but replacing `diskbb` to the relativistic disk emission model `kerrbb` (Li et al. 2005). In this fit, we allowed the mass accretion rate and M_{BH} to vary and fixed all the other parameters of `kerrbb`: $f_{\text{col}} = 1.7$, $i = 70^\circ$ or 85° , $D = 8 \text{ kpc}$, $a_* = 0$, where a_* is the dimensionless spin parameter of the black hole defined as Jc/GM^2 (J is the angular momentum of the black hole). We assumed a torque-free inner boundary and considered the self-irradiation effect but ignored the limb-darkening effect. From this model, M_{BH} was estimated to be $6.1_{-0.3}^{+0.4}$ and $10.5_{-0.5}^{+0.7}$ for $i = 70^\circ$ and 85° , respectively. These values, although having large errors, are consistent with the values that we obtained from the `diskbb` model, and hence the relativistic effects can be considered to be weak in a non-rotating black hole.

In the case of a Kerr black hole with a prograde spin, the relativistic effects can be stronger because the ISCO radius decreases with the spin, and the observed disk spectrum can significantly deviate from what `diskbb` predicts. Generally, the black hole mass estimated from the relativistic disk model increases as the spin increases

and the ISCO radius decreases, but the exact value depends on the black hole spin and the inclination angle in a complicated way (e.g., Shidatsu et al. 2011; Wang et al. 2018). Estimating the black hole mass and spin and the inclination simultaneously is difficult for the MAXI/GSC data, due to insufficient statistics and lack of data in the soft X-ray band below 2 keV. Application of the relativistic disk model to a better quality soft X-ray spectra is left as a future work.

In Figure 9 we plotted the M_{BH} versus D relation obtained above. While the inclination angle of MAXI J1803–298 is likely to be $i \gtrsim 70^\circ$ because of the presence of winds and absorption dips, the distance have not been constrained so far. Considering the luminosity at the soft X-ray peak (MJD 59350) was likely close to the Eddington luminosity (see Section 5.2), we can get another constraint on M_{BH} and D . This is also plotted in Fig. 9. Here, the unabsorbed 0.01–100 keV flux at the soft X-ray peak, $2.4 \times 10^{-8} \text{ erg cm}^{-2} \text{ s}^{-1}$, was adopted and was converted to the luminosity L_{peak} by assuming emission from a geometrically thin disk surface.

Combination of the D versus M_{BH} relations from the ISCO radius and peak luminosity favors moderate or large distances, $\gtrsim 11 \text{ kpc}$ for $i = 70^\circ$, and $\gtrsim 6 \text{ kpc}$ for $i = 85^\circ$ when $L_{\text{peak}} > 0.5L_{\text{Edd}}$ is assumed. The source is therefore likely located near the galactic center or farther. This is in agreement with the fact that the absorption column density estimated with a NICER spectrum is consistent with the total Galactic column $N_{\text{H}} \sim 3 \times 10^{21} \text{ cm}^{-2}$ obtained from the ftool `nh`, which calculates the hydrogen column density based on the 2D HI4PI map, a full-sky HI survey (HI4PI Collaboration et al. 2016). A relatively large black hole mass $\gtrsim 8M_{\odot}$ was obtained in either case of the inclination angles.

6. SUMMARY

Using the MAXI/GSC and *Swift*/BAT data, we have studied the X-ray spectral evolution of the new Galactic black hole candidate MAXI J1803–298. The source showed the state transition from the low/hard state to the high/soft state via the intermediate state. The flux variation on timescale of ~ 1 day was detected in the intermediate state, which could be interpreted as a rapid change in the mass accretion rate (and possibly launch of a Compton-thick outflow) at the transition between the standard disk and the slim disk. Using the inner disk radius in the high/soft state and the peak luminosity, we estimated a black hole mass and distance of MAXI J1803–298 to be $\sim 8M_{\odot}$ and $\gtrsim 6 \text{ kpc}$ (where a non-spinning black hole, an inclination of $\gtrsim 70^\circ$, and

the peak luminosity of $\gtrsim 0.5$ times the Eddington luminosity are assumed), suggesting that the source is a

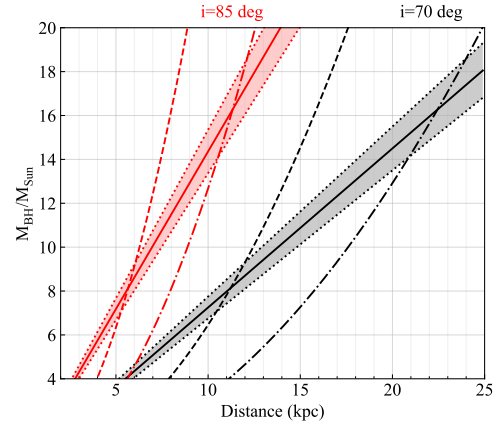


Figure 9. Constraints on the black hole mass and distance of MAXI J1803–298 for an inclination of 70° (black) and 85° (red), where a Schwarzschild black hole is assumed. The solid lines are derived from the inner disk radius in the high/soft state, and the shadowed region are their 90% error ranges. The dashed and dash-dotted lines show the relations obtained when the peak luminosity is 0.5 and 1.0 L_{Edd} , respectively.

black hole X-ray binary located near or farther than the galactic center region.

ACKNOWLEDGMENTS

This work made use of MAXI data provided by RIKEN, JAXA, and the MAXI team, and from Data ARchives and Transmission System (DARTS) at ISAS/JAXA, and of *Swift* public data from the *Swift* data archive. Part of this work was financially supported by Grants-in-Aid for Scientific Research 19K14762 (MS) from the Ministry of Education, Culture, Sports, Science and Technology (MEXT) of Japan.

Facilities: MAXI (GSC), *Swift* (BAT), NICER (XTI)

Software: XSPEC (v12.11.1; Arnaud 1996), HEASoft (v6.28; HEASARC 2014)

REFERENCES

- Arnaud, K. A. 1996, in *Astronomical Society of the Pacific Conference Series*, Vol. 101, *Astronomical Data Analysis Software and Systems V*, ed. G. H. Jacoby & J. Barnes, 17
- Buckley, D. A. H., Brink, J., Charles, P. A., & Groenewald, D. 2021, *The Astronomer's Telegram*, 14597, 1
- Bult, P. M., Gendreau, K. C., Enoto, T., et al. 2021, *The Astronomer's Telegram*, 14602, 1
- Chand, S., Dewangan, G. C., Thakur, P., Tripathi, P., & Agrawal, V. K. 2021, *The Astronomer's Telegram*, 14630, 1
- Chenevez, J., Maartensson, A. S., Andersen, C. L., & Jaisawal, G. K. 2021, *The Astronomer's Telegram*, 14601, 1
- Davis, S. W., Blaes, O. M., Hubeny, I., & Turner, N. J. 2005, *ApJ*, 621, 372, doi: [10.1086/427278](https://doi.org/10.1086/427278)
- Ebisawa, K., Makino, F., Mitsuda, K., et al. 1993, *ApJ*, 403, 684, doi: [10.1086/172239](https://doi.org/10.1086/172239)
- Espinasse, M., Carotenuto, F., Tremou, E., et al. 2021, *The Astronomer's Telegram*, 14607, 1
- Feng, Y., Zhao, X., Li, Y., et al. 2021, arXiv e-prints, arXiv:2112.02794. <https://arxiv.org/abs/2112.02794>
- Gendreau, K., Arzoumanian, Z., Enoto, T., et al. 2021, *The Astronomer's Telegram*, 14588, 1
- Gierliński, M., & Done, C. 2003, *MNRAS*, 342, 1083, doi: [10.1046/j.1365-8711.2003.06591.x](https://doi.org/10.1046/j.1365-8711.2003.06591.x)
- Gropp, J. D., Kennea, J. A., Lien, A. Y., et al. 2021, *The Astronomer's Telegram*, 14591, 1
- HEASARC. 2014, HEASoft: Unified Release of FTOOLS and XANADU, *Astrophysics Source Code Library*. <http://ascl.net/1408.004>
- HI4PI Collaboration, Ben Bekhti, N., Flöer, L., et al. 2016, *A&A*, 594, A116, doi: [10.1051/0004-6361/201629178](https://doi.org/10.1051/0004-6361/201629178)
- Homan, J., Gendreau, K. C., Sanna, A., et al. 2021, *The Astronomer's Telegram*, 14606, 1
- Hori, T., Ueda, Y., Shidatsu, M., et al. 2014, *ApJ*, 790, 20, doi: [10.1088/0004-637X/790/1/20](https://doi.org/10.1088/0004-637X/790/1/20)
- Hosokawa, R., Murata, K. L., Niwano, M., et al. 2021, *The Astronomer's Telegram*, 14594, 1
- Jana, A., Jaisawal, G. K., Chhotaray, B., et al. 2021, *The Astronomer's Telegram*, 14629, 1
- Kubota, A., & Makishima, K. 2004, *ApJ*, 601, 428, doi: [10.1086/380433](https://doi.org/10.1086/380433)
- Kubota, A., Tanaka, Y., Makishima, K., et al. 1998, *PASJ*, 50, 667, doi: [10.1093/pasj/50.6.667](https://doi.org/10.1093/pasj/50.6.667)
- Kuulkers, E., Kouveliotou, C., Belloni, T., et al. 2013, *A&A*, 552, A32, doi: [10.1051/0004-6361/201219447](https://doi.org/10.1051/0004-6361/201219447)
- Li, L.-X., Zimmerman, E. R., Narayan, R., & McClintock, J. E. 2005, *ApJS*, 157, 335, doi: [10.1086/428089](https://doi.org/10.1086/428089)
- Maccarone, T. J. 2003, *A&A*, 409, 697, doi: [10.1051/0004-6361:20031146](https://doi.org/10.1051/0004-6361:20031146)
- Mata Sánchez, D., Muñoz-Darias, T., Cúneo, V. A., et al. 2022, arXiv e-prints, arXiv:2201.09896. <https://arxiv.org/abs/2201.09896>
- Matsuoka, M., Kawasaki, K., Ueno, S., et al. 2009, *PASJ*, 61, 999, doi: [10.1093/pasj/61.5.999](https://doi.org/10.1093/pasj/61.5.999)
- McClintock, J. E., & Remillard, R. A. 2006, *Black hole binaries*, Vol. 39, 157–213
- Miller, J. M., & Reynolds, M. T. 2021, *The Astronomer's Telegram*, 14650, 1
- Mitsuda, K., Inoue, H., Koyama, K., et al. 1984, *PASJ*, 36, 741
- Miyamoto, S., Kitamoto, S., Hayashida, K., & Egoshi, W. 1995, *ApJL*, 442, L13, doi: [10.1086/187804](https://doi.org/10.1086/187804)
- Morii, M., Kawai, N., Sugimori, K., et al. 2010, in *American Institute of Physics Conference Series*, Vol. 1279, *Deciphering the Ancient Universe with Gamma-ray Bursts*, ed. N. Kawai & S. Nagataki, 391–393, doi: [10.1063/1.3509322](https://doi.org/10.1063/1.3509322)
- Nakahira, S., Ebisawa, K., Negoro, H., Mihara, T., & Sugizaki, M. 2013, *Journal of Space Science Informatics*, 2, 29
- Negoro, H., Kohama, M., Serino, M., et al. 2016, *PASJ*, 68, S1, doi: [10.1093/pasj/psw016](https://doi.org/10.1093/pasj/psw016)
- Neilsen, J., Rahoui, F., Homan, J., & Buxton, M. 2016, *ApJ*, 822, 20, doi: [10.3847/0004-637X/822/1/20](https://doi.org/10.3847/0004-637X/822/1/20)
- Saikia, P., Russell, D. M., Baglio, M. C., Bramich, D. M., & Lewis, F. 2021, *The Astronomer's Telegram*, 14706, 1
- Serino, M., Negoro, H., Nakajima, M., et al. 2021, *The Astronomer's Telegram*, 14587, 1
- Sguera, V., & Sidoli, L. 2021, *The Astronomer's Telegram*, 14598, 1
- Shidatsu, M., Done, C., & Ueda, Y. 2016, *ApJ*, 823, 159, doi: [10.3847/0004-637X/823/2/159](https://doi.org/10.3847/0004-637X/823/2/159)
- Shidatsu, M., Ueda, Y., Nakahira, S., et al. 2011, *PASJ*, 63, S803, doi: [10.1093/pasj/63.sp3.S803](https://doi.org/10.1093/pasj/63.sp3.S803)
- Shidatsu, M., Negoro, H., Kawai, N., et al. 2021, *The Astronomer's Telegram*, 14627, 1
- Shimura, T., & Takahara, F. 1995, *ApJ*, 445, 780, doi: [10.1086/175740](https://doi.org/10.1086/175740)
- Steiner, J. F., McClintock, J. E., Remillard, R. A., et al. 2010, *ApJL*, 718, L117, doi: [10.1088/2041-8205/718/2/L117](https://doi.org/10.1088/2041-8205/718/2/L117)
- Steiner, J. F., Narayan, R., McClintock, J. E., & Ebisawa, K. 2009, *PASP*, 121, 1279, doi: [10.1086/648535](https://doi.org/10.1086/648535)
- Steiner, J. F., U. S. T. J. A. C. B. H. J. 2021, *The Astronomer's Telegram*, 14994, 1
- Sugizaki, M., Mihara, T., Serino, M., et al. 2011, *PASJ*, 63, S635, doi: [10.1093/pasj/63.sp3.S635](https://doi.org/10.1093/pasj/63.sp3.S635)

- Tamura, M., Kubota, A., Yamada, S., et al. 2012, *ApJ*, 753, 65, doi: [10.1088/0004-637X/753/1/65](https://doi.org/10.1088/0004-637X/753/1/65)
- Ubach, S., Steiner, J., Homan, J., et al. 2021, *The Astronomer's Telegram*, 14660, 1
- Vahdat Motlagh, A., Kalemci, E., & Maccarone, T. J. 2019, *MNRAS*, 485, 2744, doi: [10.1093/mnras/stz569](https://doi.org/10.1093/mnras/stz569)
- Wang, S., Kawai, N., Shidatsu, M., et al. 2018, *PASJ*, 70, 67, doi: [10.1093/pasj/psy058](https://doi.org/10.1093/pasj/psy058)
- Wang, Y., Xu, Y., Ji, L., et al. 2021, *The Astronomer's Telegram*, 14613, 1
- Wilms, J., Allen, A., & McCray, R. 2000, *ApJ*, 542, 914, doi: [10.1086/317016](https://doi.org/10.1086/317016)
- Xu, Y., & Harrison, F. 2021, *The Astronomer's Telegram*, 14609, 1
- Zdziarski, A. A., Johnson, W. N., & Magdziarz, P. 1996, *MNRAS*, 283, 193, doi: [10.1093/mnras/283.1.193](https://doi.org/10.1093/mnras/283.1.193)
- Życki, P. T., Done, C., & Smith, D. A. 1999, *MNRAS*, 309, 561, doi: [10.1046/j.1365-8711.1999.02885.x](https://doi.org/10.1046/j.1365-8711.1999.02885.x)

APPENDIX

A. MAXI/GSC FOLODED SPECTRA IN THE INDIVIDUAL PHASES

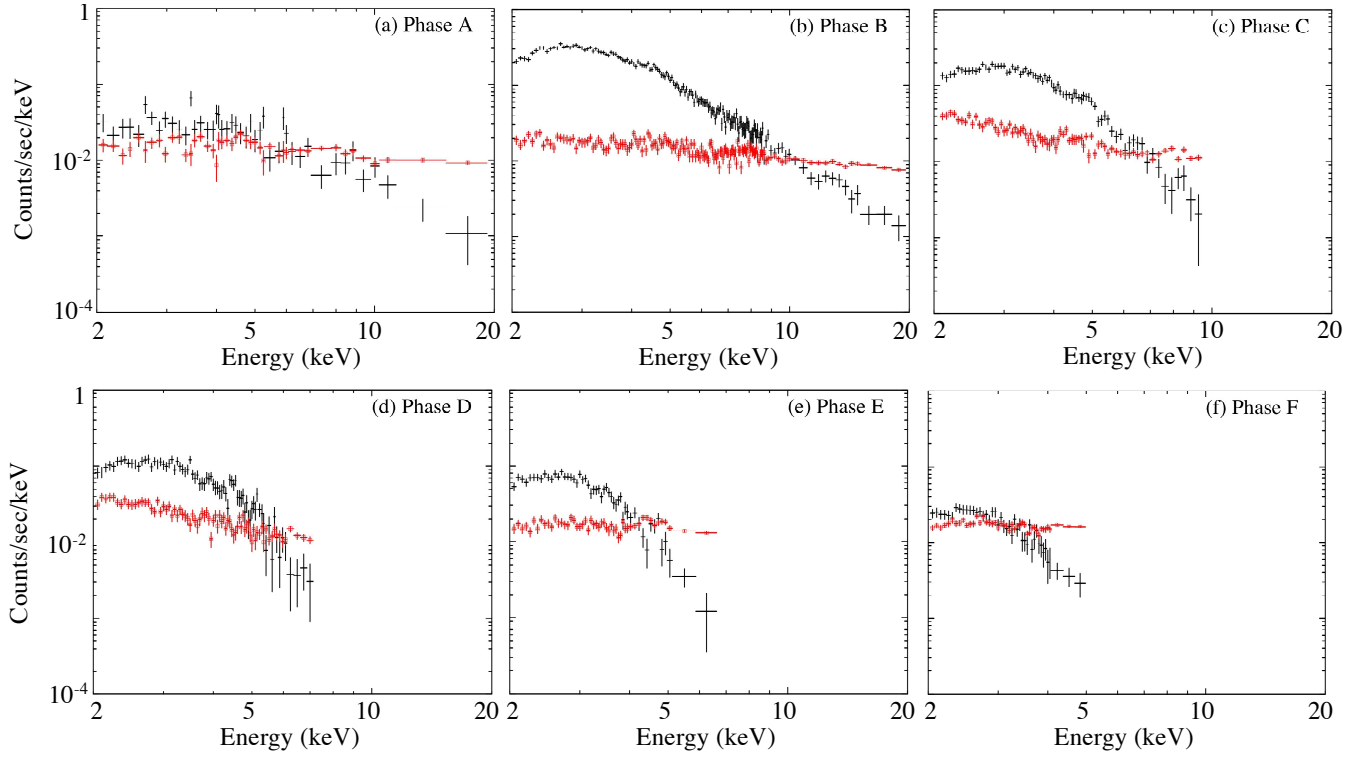


Figure 10. The MAXI/GSC response-folded, background-subtracted spectrum of MAXI J1803–298 in Phase A–F. The background spectra are shown with red open squares.